ENGINEERING

Biochemically functionalized probes for cell-type–specific targeting and recording in the brain

Anqi Zhang[1,2]†, Theodore J. Zwang[2,3,4]†, Charles M. Lieber[2]*‡

Selective targeting and modulation of distinct cell types and neuron subtypes is central to understanding complex neural circuitry and could enable electronic treatments that target specific circuits while minimizing off-target effects. However, current brain-implantable electronics have not yet achieved cell-type specificity. We address this challenge by functionalizing flexible mesh electronic probes, which elicit minimal immune response, with antibodies or peptides to target specific cell markers. Histology studies reveal selective association of targeted neurons, astrocytes, and microglia with functionalized probe surfaces without accumulating off-target cells. In vivo chronic electrophysiology further yields recordings consistent with selective targeting of these cell types. Last, probes functionalized to target dopamine receptor 2 expressing neurons show the potential for neuron-subtype–specific targeting and electrophysiology.

INTRODUCTION

A central step in deciphering complex brain circuits is to identify the roles of specific cell types and neural subtypes (*1*–*4*). The ability to target specific cell types for recording and modulation is critical to achieving this goal. With the advent of optogenetics (*5*), for example, specific cell types can be engineered such that they express light-sensitive channelrhodopsins (*6*), thereby enabling targeted optogenetic stimulation. However, cell-type–specific recording and modulation has not been possible with implantable electrical probes. Traditional probes made of silicon, for example, have substantially higher stiffness than soft brain tissue and larger feature size than individual neurons, which can lead to chronic immune response including buildup of glial scar tissue and depletion of neurons immediately adjacent to electrodes (*7*, *8*). Considerable effort has been placed on increasing substrate flexibility and reducing feature size (*7*–*11*) to address the chronic immune response. For example, mesh electronic probes (*12*–*14*), which were designed with tissue-like flexibility and a macroporous structure, do not elicit inflammatory immune response and show little effect on the natural distribution of neurons and glial cells after implantation. The minimal immune response makes them an attractive substrate for functionalization with antibodies or peptides targeting specific cell types or neural subtypes, which might allow for selective in vivo electrophysiology without genetic modification.

Previously, surface modification approaches have been used to functionalize the surfaces of chip-based electrodes and nanoprobes for cellular measurements (*15*–*19*). For example, attachment of Arg-Gly-Asp (RGD)-based peptides that trigger adhesion and engulfment mechanisms have been shown to yield intracellular-like recording with mushroom-like gold electrodes (*16*), while phospholipid layers on the surfaces of nanoscale transistor probe arrays facilitated internalization and intracellular recording in primary neurons and cardiac cells (*17*–*19*). In addition, substantial work has been carried out functionalizing the surfaces of implanted neural probes with biologically derived or biomimetic materials (*20*, *21*), including neuronal cell adhesion molecules, extracellular matrix molecules, and conductive polymers. These biocompatible surface coatings effectively reduced the immune response and promoted neuronal survival adjacent to the neural probes but have not shown the capability to target and monitor specific cell types.

RESULTS

Implantable mesh probes with cell-type specificity

Mesh electronic probes were first modified with either a control antibody or antibodies and peptides that can recognize specific surface receptors of different cell types, including neurons, astrocytes, and microglia (Fig. 1A). To target neurons, we selected the peptide sequence Ile-Lys-Val-Ala-Val (IKVAV), a fragment of laminin α-1 that has been demonstrated to promote neuronal cell attachment on substrates while minimizing glial cell adhesion (*22*–*24*). To target astrocytes, we chose an antibody targeting the extracellular domain of excitatory amino acid transporter 2 (EAAT2), a membrane-targeted glutamate transporter highly expressed in mature astrocytes (*25*). To target microglia, we chose an antibody targeting the microglia surface marker CD11b (*26*). To exclude the possible effects of immune response (i.e., accumulation of astrocytes and microglia) induced by foreign antibodies anti-EAAT2 and anti-CD11b, we included a rabbit anti-human immunoglobulin G (IgG) antibody as a negative control (control Ab) because it was produced in the same host species and does not specifically bind to cells in the mouse brain.

The probes (fig. S1) consist of double-sided platinum electrodes (*27*) embedded in the polymer-based mesh-like region and connected through a stem to the input/output (I/O) structure that provides an electrical interface for external recording as described previously (*28*). Surface functionalization of the mesh region is based on standard covalent coupling chemistry (*29*) that uses the carboxyl (−COOH) groups on the surface of the SU-8 polymer resulting from the oxygen plasma treatment at the end of probe fabrication (*30*) using 1-ethyl-3-(3-dimethylaminopropyl)

[1]Department of Chemical Engineering and Department of Bioengineering, Stanford University, Stanford, CA 94305, USA. [2]Department of Chemistry and Chemical Biology, Harvard University, Cambridge, MA 02138, USA. [3]MassGeneral Institute for Neurodegenerative Disease, Massachusetts General Hospital, Boston, MA 02114, USA. [4]Department of Neurology, Harvard Medical School, Boston, MA 02114, USA.
*Corresponding author. Email: liebercharlesm@gmail.com
†These authors contributed equally to this work.
‡Present address: Lieber Research Group, Lexington, MA, USA.

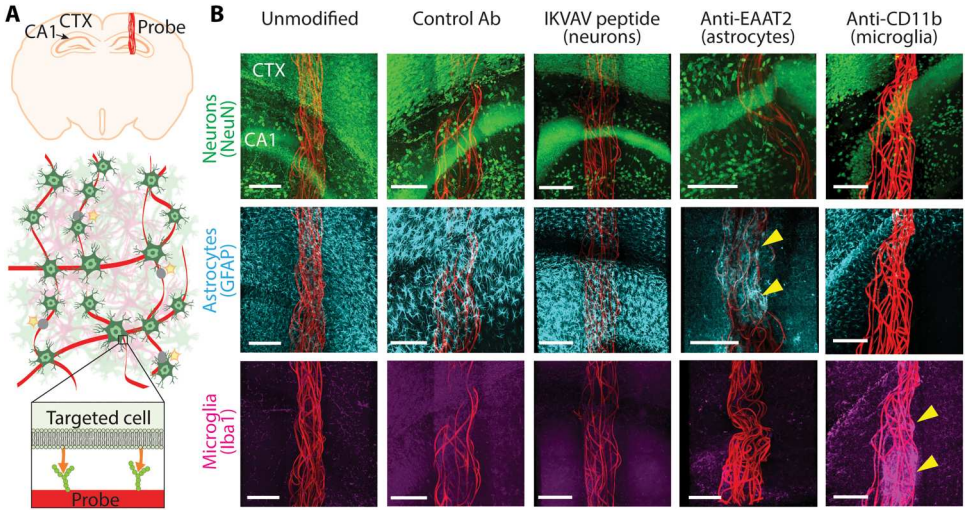

Fig. 1. Implanted control and functionalized mesh probes. (**A**) Top: Schematic of a coronal brain section showing a mesh probe (red) implanted through the cortex (CTX) into the mouse hippocampus with the cornu ammonis (CA1) region indicated. Bottom: Schematics of small volumes of brain tissue/probe interface highlighting probes functionalized with antibodies and peptides capable of targeting specific cell types. Mesh probe ribbons are in red, electrodes are in gray. Cells in green are targeted cells; cells in pink are nontargeted cells. (**B**) Representative fluorescence images of coronal mouse brain section of control and functionalized probes including the hippocampal CA1 region 14 days after implantation. The five columns correspond to an unmodified probe as well as four distinct probes functionalized with either control antibody (Ab), IKVAV peptide for targeting neurons, anti-EAAT2 for targeting astrocytes, or anti-CD11b for targeting microglia. The three rows highlight the tissue staining of the section (across the five distinct probe modifications) with NeuN, GFAP, and Iba1 antibodies for neurons, astrocytes, and microglia, respectively. The yellow triangles in the anti-EAAT2–GFAP and anti-CD11b–Iba1 panels highlight the specific targeting of astrocytes and microglia, respectively. Scale bars, 200 μm.

carbodiimide (EDC)/*N*-hydroxysuccinimide (NHS) (*29*). The EDC/NHS covalent biomolecule conjugation to surfaces is a well-established methodology for stable immobilization of proteins and other biomolecules (*31*). The modification process was carried out by first loading probes into glass capillary tubes and then dipping the end closer to the mesh region into the respective modification solutions (see Materials and Methods). The primary amine ($-NH_2$) groups on the peptides and primary antibodies are covalently coupled to the −COOH groups on the probe surface using EDC/NHS (*29*). The effectiveness of the coupling was characterized by confocal fluorescence microscopy where either fluorophore-labeled IKVAV peptides were directly coupled or secondary antibodies were incubated with the conjugated primary antibodies (fig. S2). The images show uniform fluorescence on the SU-8 polymer ribbons consistent with specific modifications of the probe surface without aggregates of either the peptide or the antibody layers.

The unmodified and functionalized probes were implanted into the mouse hippocampus using a stereotaxic injection method (Fig. 1A) (*32*). Fourteen days after implantation, the brains were extracted, sectioned, cleared, and stained using a modified CLARITY (*33*) protocol (see Materials and Methods) to allow fluorescence imaging of the cellular environment around the intact probe. We labeled the brain tissue with antibodies for neurons (anti-NeuN), astrocytes [anti–glial fibrillary acidic protein (GFAP)], and microglia [anti-ionized calcium binding adaptor molecule 1 (Iba1)] and used confocal microscopy to image the hippocampal CA1 region in 1-mm-thick tissue sections containing the intact probes. We observed notable differences in the cellular environments near probes with different modifications (Fig. 1B). For unmodified, control Ab–modified, and IKVAV peptide–modified mesh probes, neuron somas and axons fully penetrated the probe ribbons, with neurons, astrocytes, and microglia exhibiting similar distribution inside and outside the mesh boundaries. The anti-EAAT2– and anti-CD11b–modified mesh probes, however, showed substantially enhanced accumulation of astrocytes and microglia, respectively. Qualitative comparison of how the different probe surfaces affected cell distributions reveals several important points. First, the similar cell distribution near unmodified, control Ab–modified, and IKVAV peptide–modified mesh probes indicates that antibodies produced in different species (e.g., rabbit) did not cause a substantial immune response within the observed 14-day time frame and that the modification strategy did not have an adverse effect on the intrinsic biocompatibility of the mesh probes. Second, the anti-EAAT2– and anti-CD11b–modified probes selectively attracted astrocytes and microglia, respectively, without affecting off-target cell types, which confirmed our initial hypothesis that the surface functionalization with specific antibodies could selectively recruit different cell types. Third, the accumulated cells were only observed near the surface of the mesh ribbons, indicating that the modifications only affected cells close to the functionalized probes.

We then asked whether quantitative analyses of modified probes implanted into mouse brains could provide more insight into these qualitative observations as well as the potential for recruitment of neurons by examination of time-dependent histology data (Fig. 2 and figs. S3 to S9). Histology imaging was replicated on samples (at least $n = 3$ mice at each time point) containing mesh probes with different modifications on days 3, 7, and 14 after implantation (Fig. 2, A to C, and figs. S3 and S4). We identified individual neurons, astrocytes, and microglia in the CA1 region using reported methods (*34*, *35*) and then plotted the different cell density distributions up to 300 μm away from the probe surface (see Materials and Methods, Fig. 2, D to F, and figs. S3 and S4). The cell density was compared quantitatively by binning all cells at a given distance

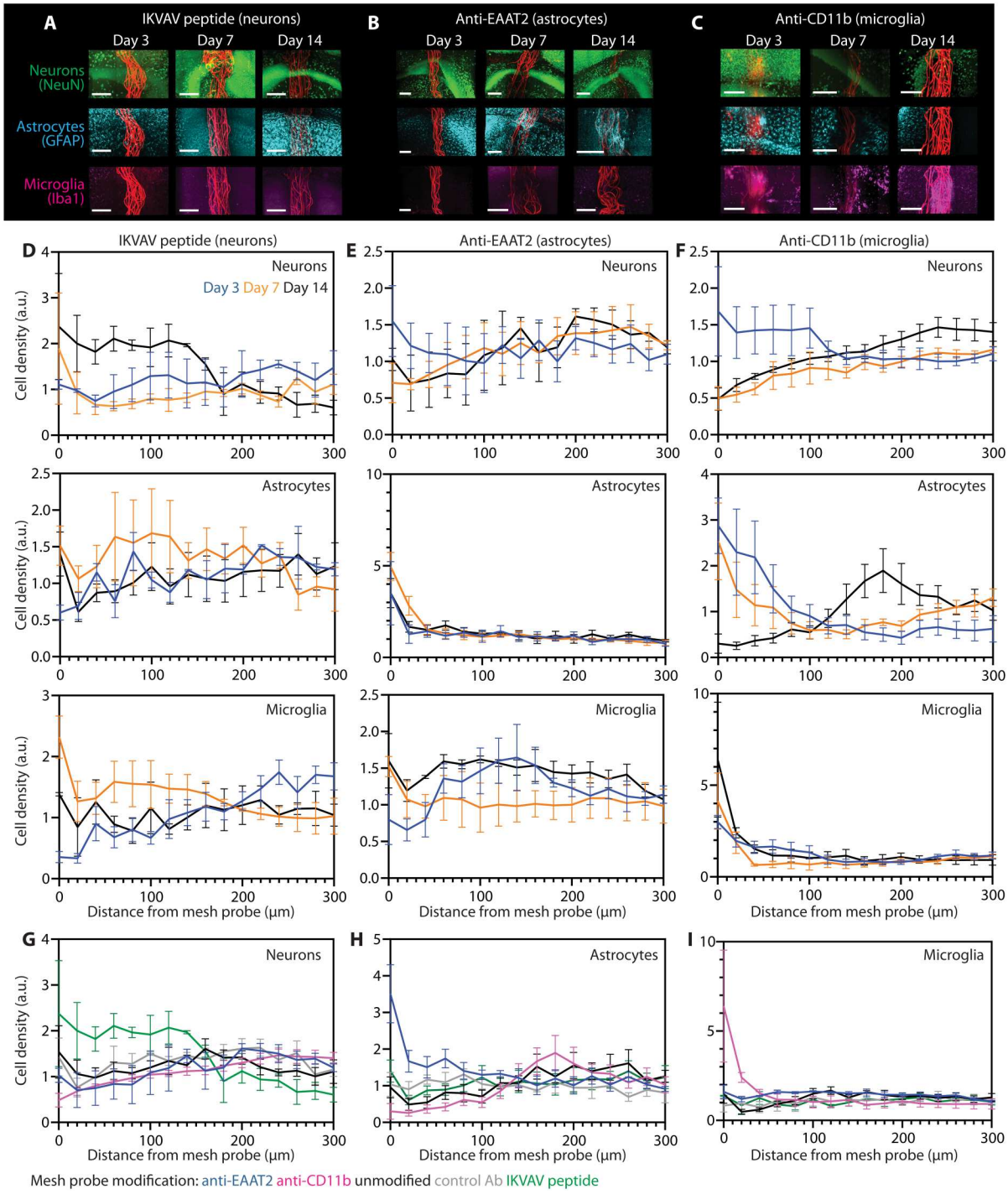

Fig. 2. Time-dependent histology studies of mesh probe–brain interfaces. (**A** to **C**) Time-dependent confocal microscopy images of cleared tissue slices at 3, 7, and 14 days after implantation labeled with NeuN (neurons; top), GFAP (astrocytes; middle), and Iba1 (microglia; bottom) for mesh probes functionalized with (A) IKVAV peptide, (B) anti-EAAT2, and (C) anti-CD11b. Scale bars, 200 μm. (**D** to **F**) Normalized cell density distribution for neurons (top), astrocytes (middle), and microglia (bottom) in the CA1 region as a function of distance from surface of mesh probes modified with (D) IKVAV peptide, (E) anti-EAAT2, and (F) anti-CD11b on days 3 (blue), 7 (orange), and 14 (black) (at least $n = 3$ mice at each time point). (**G** to **I**) Normalized cell density distribution for (G) neurons, (H) astrocytes, and (I) microglia as a function of distance from the probes modified with anti-EAAT2 (blue), anti-CD11b (pink), unmodified (black), control antibody (gray), and IKVAV peptide (green) 14 days after implantation. Values are means ± SEM. See figs. S5 to S9 for cell density distribution plots for individual samples. a.u., arbitrary units.

from the probe surface. Each value from a given sample was normalized to the average value from all bins in that sample.

Consistent with our previous observations, the unmodified (fig. S3) (*14*) and control Ab–modified mesh probes (fig. S4) only showed a small displacement of neurons near the probe surface that recovered over time and no major influence on the distribution of astrocytes or microglia. Notably, the other probes showed different time courses of cellular accumulation depending on their surface modifications. For IKVAV peptide–modified mesh probes (Fig. 2D), the neuron density increased 14 days after implantation, while the density of astrocytes and microglia always remained consistent with the baseline as with the control Ab. For probes modified with anti-EAAT2 (Fig. 2E), an increased density of astrocytes was observed at all time points near the mesh surface, while the microglia density remained close to the baseline level and the neuron density slightly decreased approaching the probe surface. For probes modified with anti-CD11b (Fig. 2F), there was an accumulation of microglia near the probes at all time points, the astrocyte density temporarily increased on day 3 and dropped below the baseline on day 14, and the neuron density decreased when approaching the probe surface. A summary of the distributions of neurons, astrocytes, and microglia adjacent to mesh probes with different modifications 14 days after implantation (Fig. 2, G to I) further highlights the specific targeting of neurons, astrocytes, and microglia by the IKVAV peptide–, anti-EAAT2–, and anti-CD11b–modified mesh probes, respectively. These observations demonstrate two important points. First, the specific accumulation of microglia and astrocytes occurred at a faster rate than that of the neurons, consistent with the higher mobility and enhanced migration of microglia and astrocytes than neurons after acute brain injury (*36*). Second, during recovery, astrocytes and microglia would selectively accumulate near the probe surface depending on the modification, suggesting that the process was driven by modification rather than generalized inflammation where both cell types are expected to accumulate (*36*).

Cell-type–specific electrophysiological recording

Next, we asked how the specific targeting of different cell types affects electrophysiology recording. Because the neuron spike amplitude recorded by extracellular electrodes decreases exponentially with distance from the electrode (*37*), we hypothesized that IKVAV peptide–modified probes should show an increase in the number of recorded neurons and an increase in mean spike amplitudes, while anti-EAAT2– and anti-CD11b–modified mesh probes would show a decrease in both quantities, compared to unmodified and control Ab–modified mesh probes.

Probes with different surface functionalizations (n = 3 mice for each condition) were implanted through the cortex and into the hippocampus of mice for in vivo chronic recording measurements. Multiplexed recordings from head-fixed, awake mice (Fig. 3, A to C, and fig. S10) exhibited stable single-unit spikes from the time of initial implantation to the endpoint of the measurements (days 1 to 14; figs. S11, S13, S15, S17, and S19). Single-neuron activity was tracked by clustering the sorted spikes with principal components analysis from all channels as a function of time (figs. S12, S14, S16, S18, and S20) (*12*). These recordings highlight several key points. First, the IKVAV peptide–modified and unmodified mesh probes showed more single-unit spikes than the anti-CD11b– and anti-EAAT2–modified mesh probes. Second, the control Ab–modified probes showed a similar level of spontaneous firing to that recorded by the unmodified probes. Third, the number of distinct neurons detected, represented by different color waveforms, increased mainly within the first 7 days, consistent with our previous results with unmodified mesh probes (*14*).

We carried out statistical analyses of the sorted spikes from the probes with different modifications (Fig. 3, D and E, and fig. S21) to better understand these results. The average numbers of distinct neurons recorded per electrode from probes with different modifications (Fig. 3D) showed a significant increase for the IKVAV peptide–modified probes and a significant decrease for the anti-CD11b– and anti-EAAT2–modified probes. In addition, the control Ab–modified probes appear to have recorded similar numbers of neurons as the unmodified probes. To specifically examine the number of neurons closely associated with the probe surface, we compared the amplitudes of all recorded neurons and set the amplitude threshold for close association as the means + SD (49.5 + 14.3 mV) because the spike amplitude decreases in an exponential manner as the distance from the electrode increases (Fig. 3E) (*37*). Fourteen days after implantation, the IKVAV peptide–modified mesh probes recorded significantly higher numbers of closely associated neurons, while both anti-CD11b and anti-EAAT2 mesh probes showed significantly lower numbers of such neurons. These analyses are consistent with our quantitative histology data that showed IKVAV peptide–functionalized probes enhanced neuron density close to the surface, while the accumulation of microglia and astrocytes excluded neurons adjacent to the anti-CD11b– and anti-EAAT2–modified probes. The similarity of electrophysiology results between unmodified and control Ab–modified mesh probes further supports our assessment that the antibody modification itself does not provoke an immune response and that antibodies are changing the cell distribution by associating with their respective membrane surface antigens.

Targeting a neuron subtype

Last, we asked whether functionalized probes could be exploited to target different neuron subtypes. We modified probes with an antibody that binds to an extracellular region of dopamine receptor 2 (D2R) to distinguish D2R-expressing neurons from the general population of neurons. Representative staining of D2R neurons in tissue sections with D2R antibody (D2R Ab)–modified (Fig. 4A) and unmodified mesh probes (Fig. 4B) near the CA1 region showed an increased association of D2R neurons with the D2R Ab–modified probes that also extend into the sub-CA1 regions without endogenous D2R neurons (Fig. 4, A and B, yellow dashed boxes). The small number of D2R neurons detected in the sub-CA1 region of the D2R Ab–modified probes is consistent with trapping of D2R-expressing newborn neurons migrating from the dentate gyrus (*38*). The specific targeting of D2R neurons was confirmed by plotting the normalized D2R neuron density near the probe surface in the CA1 region (Fig. 4C and fig. S22).

Intracortical injection of 20 μg of D2R antagonist eticlopride (ETIC), which specifically increases the firing frequency of neurons with D2R (*39*, *40*), was used to confirm the targeting of D2R neurons in electrophysiology recording. Injections were carried out ca. 1.5 mm away from the implanted mesh probes. The neural activity was recorded from mice under stable anesthesia for 20 min before and 30 min after ETIC injection to allow sufficient diffusion, from mesh probes with and without D2R Ab

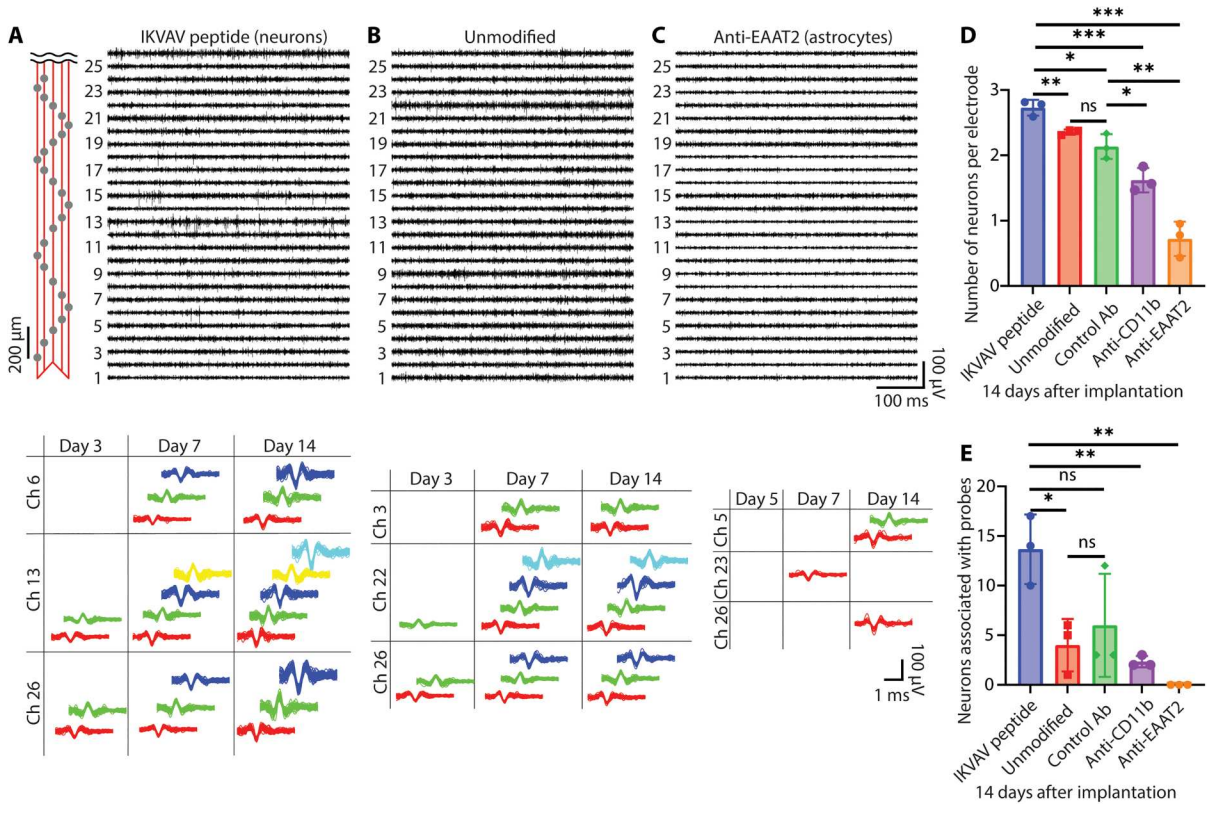

Fig. 3. Cell-type–specific electrophysiological recording and analysis. (**A** to **C**) Top: Representative 26-channel single-unit spike traces 14 days after implantation from mesh probes modified with IKVAV peptide for targeting neurons (A), unmodified (B), and modified with anti-EAAT2 for targeting astrocytes (C). Recordings were made from head-fixed, awake mice. The *x* and *y* axes represent recording time and voltage, respectively. The relative positions of the recording electrodes are marked by gray dots in the schematic (leftmost panel). Channels with smaller numbers are implanted deeper. Bottom: Time evolution principal components analysis clustered single-unit spikes from three representative channels. For each channel, each distinct color in the sorted spikes represents a unique identifiable neuron. (**D**) Average number of distinct neurons recorded per electrode 14 days after implantation from mesh probes with different modifications ($n = 3$ mice). (**E**) Number of detected neurons closely associated with probes for the different modifications 14 days after implantation ($n = 3$ mice). Close association of recorded neurons is defined as amplitude greater than the mean amplitude of all mesh probes + 1 SD. Values are means ± SD; ns, nonsignificant; $^{*}P \leq 0.05$, $^{**}P \leq 0.01$, and $^{***}P \leq 0.001$; two-tailed, unpaired, *t* test.

modification ($n = 3$ mice). Representative recordings from a D2R Ab mesh probe before and 30 min after ETIC injection (Fig. 4, D and E) exhibited increased numbers of single-unit spikes after ETIC injection, while the recordings from an unmodified mesh probe showed no clear difference before and after ETIC injection (fig. S23). Single-neuron activity was tracked by counting the number of sorted spikes with principal components analysis from every channel as a function of time represented by 5-min recording blocks (figs. S24 and S25). Comparison of the representative changes of neurons recorded by a D2R Ab probe (Fig. 4F) and an unmodified probe (Fig. 4G) revealed that, although the firing rate of the neurons recorded by the D2R Ab probe before ETIC injection remained constant, the firing rate after ETIC injection increased substantially and continued to increase for 30 min. The neurons recorded by the unmodified probe maintained a constant firing rate before and after ETIC injection. These changes for modified and unmodified probes are consistent with increased firing of D2R neurons trapped at the modified probe surface and not increased firing of neurons that are simply connected in a circuit to remote D2R neurons.

To further examine the selective D2R neuron detection shown in the above experiments, we analyzed all 151 neurons measured from three D2R Ab–modified probes and all 153 neurons measured from three unmodified probes and plotted the firing rate changes by comparing the recording time block with the maximum number of spikes after ETIC injection to the one with the maximum number of spikes before ETIC injection (before as baseline at 100%) (Fig. 4H). The neurons recorded by the D2R Ab–modified probes showed a significantly higher increase in the firing rate. In addition, D2R Ab–modified probes recorded 9 neurons that were not firing initially but started firing after ETIC injection, which were excluded from the ratio calculation. As histology studies showed that D2R neurons preferentially clustered near the D2R Ab–modified probe surface, we confirmed this observation with electrophysiology by comparing the ratio of the firing rate changes between probe-adjacent neurons (with firing amplitudes greater than mean amplitude + SD (32.6 + 10.7 mV for neurons recorded by D2R Ab probes and 38.9 + 22.8 mV for unmodified probes) and probe-distant neurons (with amplitudes lower than the mean) and determined that neurons closely associated to the D2R Ab–modified probes showed significantly higher frequency increase (median, 332%) after ETIC injection than neurons near the unmodified probes (median, 103%) (Fig. 4I). The neurons located further away from the D2R Ab probes (median, 112%) did not show

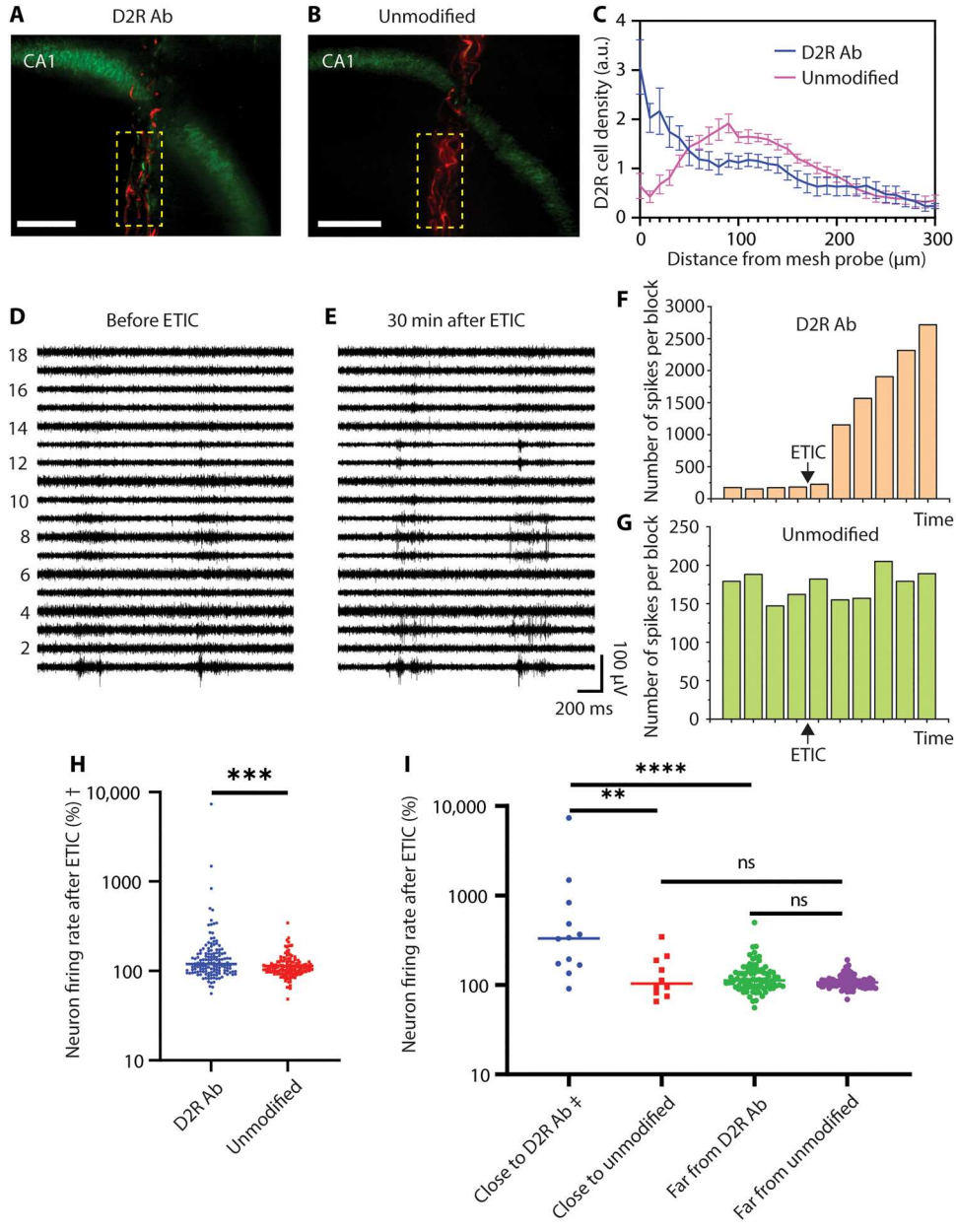

Fig. 4. Targeting a neuron subtype. (**A** and **B**) Representative fluorescence images of D2R neurons adjacent to D2R Ab–modified (A) and unmodified (B) mesh probes. The sub-CA1 regions without endogenous D2R neurons are highlighted in yellow dashed boxes. The D2R neurons are green, and the mesh probe is red. Scale bars, 200 μm. (**C**) Normalized cell density distribution for D2R neurons as a function of distance from the probes ($n = 6$ mice for D2R Ab–modified and $n = 5$ mice for unmodified). Values are means ± SEM. (**D** and **E**) Representative single-unit spike traces under anesthesia from a D2R Ab–modified probe immediately before and 30 min after ETIC injection. (**F** and **G**) Representative firing patterns of neurons recorded by D2R Ab–modified (F) and unmodified (G) probes. Black arrows denote the time of ETIC injection. Each bar represents spikes within a 5-min recording block. (**H** and **I**) Firing rate changes of neurons recorded by D2R Ab–modified and unmodified probes after ETIC injection ($n = 3$ mice). (H) All neurons († nine neurons recorded by D2R Ab probes started firing after ETIC not included); (I) neurons closely associated with probes (‡ three neurons near D2R Ab mesh probes started firing after ETIC not included) and neurons far away from probes. Values are medians; $^{**}P \leq 0.01$, $^{***}P \leq 0.001$, and $^{****}P \leq 0.0001$; two-tailed, Mann-Whitney test.

significant difference compared to those recorded by the unmodified probes (median, 106%). Together, these data demonstrate the ability to selectively target and closely associate neurons of a specific subtype to implanted electronics via binding of membrane surface antigens.

DISCUSSION

In this work, we have achieved cell-type– and neuron-subtype–specific targeting with mesh probes functionalized with specific peptides and antibodies. Chronic electrophysiological recording and time-dependent histology studies have demonstrated selective accumulation of the targeted cell types near the probe surface in a

minimally invasive, nongenetic manner. Further development of these cell-targeting capabilities could open up many opportunities in electrophysiology. First, specific modification of individual recording electrodes could trap single cells for future in vivo studies. For example, gold electrodes with sizes that are similar to that of typical neuron soma can be specifically modified by attaching biomolecules using thiol linkers (*41*). These electrodes might be able to capture a small number of specific cells or even a single cell, thereby helping to elucidate how the targeted cells integrate into local circuits. Second, incorporation of both recording and stimulation electrodes (*12*) into the mesh probe platform with modifications targeting neuron subtypes could help to decode local excitatory/inhibitory circuits and might also allow for next level of control in therapeutic brain stimulation. Third, the probes, or more specifically the electrodes, could be functionalized with antibodies or other biomolecules that target the extracellular domains of receptors expressed in neuron subtypes other than D2R neurons. For example, it would be interesting to explore specific targeting of neurons expressing dopamine receptors 1 to 5 (D1R to D5R) and the variety of serotonin receptors (*42*). Fourth, the versatility of our cell targeting strategies might be expanded by introducing artificial functional groups on the cell surface with bio-orthogonal chemistry (*43*, *44*). Fifth, stable covalent conjugation methods are essential for stable cell association and chronic recording. In addition to amide bonds formed between carboxylic acid groups on the probe surface and amine groups on biomolecules using EDC/NHS in this work, other covalent bioconjugation methods can be explored, such as the formation of amide bonds using carbonyldiimidazole, secondary amine bonds made by the reductive amination of primary amines with aldehyde groups, triazole bonds formed with surface-conjugated dibenzocyclooctyne and azide-tagged biomolecules (*45*). We anticipate that achieving cell-type–specific targeting and electrophysiology without requiring genetic modifications will expand and complement existing work based on genetically modified organisms (*46*, *47*).

MATERIALS AND METHODS

Design and fabrication of mesh electronic probes

Mesh probes with double-sided electrodes and I/O metal regions (fig. S1) were fabricated using standard photolithography as described previously (*28*). The key steps are as follows: (i) A 100-nm-thick nickel (Ni) sacrificial layer was thermally evaporated (Sharon Vacuum Co.) onto a 75 mm diameter silicon (Si) wafer (n-type 0.005 ohm·cm, 600-nm thermal oxide, NOVA Electronic Materials). (ii) LOR 3A and S1805 (Microchem) were spin-coated at 4000 rpm for 45 s and baked at 180°C for 4 min and at 115°C for 1 min, respectively. The photoresist was patterned by photolithography with a mask aligner (SUSS MA6 mask aligner, SUSS MicroTec) and developed (MF-CD-26, MicroChem Corp.) for 1 min. Following this photolithography process, a 100-nm-thick gold (Au) bottom I/O layer was deposited by thermal evaporation (Sharon Vacuum Co.), followed by a liftoff step (Remover PG, MicroChem). (iii) The photolithography process in step (ii) was repeated to define 100-nm-thick 20-μm-diameter platinum bottom electrode regions for electron-beam evaporation (Denton Vacuum Co.), followed by a liftoff step. (iv) For the bottom-passivation layer, negative photoresist SU-8 (SU-8 2000.5; MicroChem) labeled with Lissamine rhodamine B ethylenediamine [RhBen; ~10 μg ml^{-1} (*14*); Thermo Fisher Scientific] was spin-coated on the Si wafer at 3000 rpm for 30 s, prebaked at 65°C for 1 min and 95°C for 1 min, and then patterned by photolithography with the mask aligner. After post-baking at 65°C for 1 min and 95°C for 1 min, the SU-8 resist was developed in SU-8 developer (Microchem), rinsed with isopropanol, dried, and hard baked at 185°C for 1 hour. (v) The photolithography process in step (ii) was repeated to define metal interconnects, followed by 100-nm-thick Au deposition by thermal evaporation and liftoff. (vi) The top passivation layer is then patterned using a similar procedure as in step (iv), followed by hard baking at 195°C for 1 hour. (vii) The process in step (iii) was repeated to deposit the 100-nm thick top layer of platinum electrodes. (viii) To release mesh probes, the Si wafer was cleaned with oxygen plasma (50 W, 1 min) and immersed in a Ni etchant solution comprising 40% $FeCl_3$:39% HCl:H_2O = 1:1:10 on a 50°C hot plate for 90 min. Released mesh probes were rinsed with deionized (DI) water three times and transferred to sterile 1× phosphate-buffered saline (PBS) solution (HyClone, GE Healthcare Life Sciences) before surface modification or implantation.

Surface modification

The SU-8 polymer surface of mesh probes is modified at room temperature as follows. (i) A modification solution was made by dissolving 10 mM of EDC (Sigma-Aldrich Inc.) and 75 mM of NHS (Sigma-Aldrich Inc.) in 50 mM of 2-(N-morpholino)ethanesulfonic acid (MES) (Sigma-Aldrich Inc.) buffer (pH 6). (ii) Mesh probes were transferred to PBS solution. A glass capillary tube with an inner diameter (ID) of 400 μm and outer diameter (OD) of 550 μm (Produstrial) is positioned near the I/O end of the mesh probe while it is suspended in solution. The syringe connected to the other end of the glass tube was manually retracted to draw in the mesh probe into the tube. (iii) The opening of the glass tube was gently tapped on Kimwipes (Kimtech Science) to remove the PBS solution while keeping the mesh probes attached to the inner wall. (iv) The tube end closer to the mesh region was dipped into the modification solution, and, once the solution covered the mesh region, the opposite end of the tube was covered with parafilm to prevent the modification solution from reaching the stem and I/O regions. (v) The mesh region was incubated in modification solution for 30 min, followed by rinsing in PBS three times. (vi) Peptide (50 μM) for targeting neurons [KKKAASIKVAV for histology and electrophysiology or KKKAASIKVAV-K(5FAM) for validation of surface functionalization, CPC Scientific Inc.], antibodies (50 μM) for targeting microglia (anti-CD11b; ab184307, Abcam) or astrocytes (anti-EAAT2; AGC-022, Alomone Labs), or antibodies (5 μM) for targeting neurons with D2R (anti-D2DR; sc-5303, Santa Cruz Biotechnology) or without cell-type specificity (rabbit anti-human IgG; 6145-01, SouthernBiotech) were dissolved in PBS, and steps (ii) to (iv) were repeated to incubate the mesh region in antibodies or peptide. (vii) Mesh probes were then transferred to 50 mM tris buffer (pH 8) for 30 min to quench the reaction, and the probes were then stored in PBS at 4°C. Modified probes were implanted within 1 week.

In vivo brain implantation surgery

Adult (6 to 8 weeks, 20 to 25 g) male C57BL/6J mice (000664, the Jackson Laboratory) were used in the study. All procedures were approved by the Animal Care and Use Committee of Harvard University. The animal care and use programs at Harvard University meet

the requirements of federal law (89–544 and 91–579) and National Institutes of Health (NIH) regulations and are also accredited by the American Association for Accreditation of Laboratory Animal Care. Before surgical procedures, animals were group-housed on a 12-hour:12-hour light:dark schedule in the Harvard University Biology Research Infrastructure and fed with food and water ad libitum as appropriate. Animals were housed individually after surgical procedures.

In vivo implantation of the mesh probes into mouse brains was performed using a controlled stereotaxic injection method (*32*). All metal tools in direct contact with the animal subjects were bead-sterilized (Fine Science Tools) for 1 hour before use, and all plastic tools in direct contact with the animal subjects were sterilized with 70% ethanol and rinsed with sterile DI water and sterile PBS before use. The mesh probes were sterilized with 70% ethanol followed by rinsing in sterile DI water and sterile PBS before implantation. Mice were anesthetized by intraperitoneal injection of a mixture of ketamine (75 mg kg^{-1}; Patterson Veterinary Supply) and dexdomitor (1 mg kg^{-1}; Orion). The degree of anesthesia was verified via toe pinch before surgery. A homeothermic blanket (Harvard Apparatus) was set to 37°C and placed underneath the anesthetized mouse. The anesthetized mouse was placed in a stereotaxic frame (Lab Standard Stereotaxic Instrument, Stoelting Co.) equipped with two ear bars and one nose clamp. Puralube vet ointment (Dechra Pharmaceuticals) was applied to both eyes to prevent corneal damage. Hair removal lotion (Nair, Church & Dwight) was applied to the scalp for depilation, and an alternating series of Betadine surgical scrub (Purdue Products) and 70% alcohol was applied to sterilize the depilated scalp skin. A sterile scalpel was used to make a 5-mm longitudinal incision in the scalp along the sagittal sinus. The scalp skin was resected to expose a 5 mm–by–5 mm portion of the skull.

A 1-mm-diameter burr hole was made using a dental drill (Micromotor with On/Off Pedal 110/220, Grobet USA) according to the following stereotaxic coordinates: anteroposterior, 2 mm; and mediolateral, 1.5 mm. A sterilized 0–80 set screw (McMaster-Carr Supply Company) was screwed into this burr hole to a depth of 500 μm to serve as the grounding and reference electrode. Metabond adhesive cement (Parkell) was applied to fix the screw/skull junction. Another 0.5-mm-diameter burr hole was made for the implantation of mesh probes according to the following stereotaxic coordinates: anteroposterior, −1.85 mm; mediolateral, 1.45 mm; and dorsoventral, 2.50 mm. A flat, flexible cables (FFCs; WM11484-ND, Digi-Key Electronics) with 32 conductors with a 0.50-mm pitch was attached with Metabond adhesive cement onto a head restrainer made with a three-diameter printer (Makerbot, Replicator 2x) using polylactic acid filament. The head restrainer was attached and fixed on the skull with Metabond adhesive cement, and the FFC near the cranium hole served as a substrate for I/O connection.

Mesh probes were implanted into the hippocampus using a controlled injection method. First, mesh probes were loaded into a sterile glass capillary tube with an ID of 300 μm and OD of 400 μm (Produstrial), which was inserted in a micropipette holder (1-HL-U, Molecular Devices LLC) fixed on a stereotaxic stage equipped with a motorized linear translation stage (860A motorizer and 460A linear stage, Newport) that could move the stereotaxic arm in the *z* direction with a constant preset velocity ranging from 0.05 to 0.5 mm s^{-1}. The micropipette holder was connected to a 5-ml syringe that was prefilled with PBS and mounted on a syringe pump (PHD 2000, Harvard Apparatus). The glass tube was inserted into the brain tissue to the targeted coordinates. Controlled injection was carried out by synchronizing the syringe pump with the motorized linear translation stage, with a PBS injection rate of 5 to 40 ml $hour^{-1}$ and a translational stage retraction velocity of 0.2 to 0.5 mm s^{-1}. The volumetric flow rate and needle retraction velocity were adjusted such that the mesh region right above the burr hole, which was visualized through an eyepiece camera (DCC1240C, Thorlabs), remained stationary in the field of view. The total injection volume was 10 to 40 μl over the 2.5-mm length of injection. After implantation, the mesh probe is fixed at the burr hole with Metabond adhesive cement. The 32 I/O pads were aligned with flowing DI water onto the 32 conductors on the FFC. After the I/O pads were dried, ultraviolet (UV) light glue (Visbella) was applied and cured with a handheld UV flashlight (Vansky). For mesh probe implantation for histology studies without electrophysiology recording, the scalp was closed with 3M Vetbond tissue adhesive. Triple antibiotic ointment (Water-Jel Technologies) was applied copiously on the closure.

After surgery, each mouse was returned to a cage placed on a 37°C heating pad. The activity of the mouse was monitored every hour until it was fully recovered from anesthesia. Buprenex (Buprenorphine, Patterson Veterinary Supply) analgesia was given intraperitoneally at a dose of 0.05 mg kg^{-1} body weight every 12 hours for up to 72 hours after surgery.

Histology sample preparation and immunostaining

Mice with implanted mesh probes were anesthetized and transcardially perfused with ice-cold 40 ml of PBS and 40 ml of 4% formaldehyde (Electron Microscopy Sciences) at specified times after implantation, followed by decapitation. The scalp skin was removed, and the exposed skull was ground for 10 to 20 min at 10,000 rpm using a high-speed rotary tool (Dremel). The brain was removed from the cranium and placed in 4% formaldehyde in PBS for 24 hours and then transferred to PBS for at least 24 hours. The brain was then embedded in 4% agarose (SeaPlaque agarose, Lonza) hydrogel, cut into blocks of 2 cm (length) by 2 cm (width) by 1 cm (height), and then sectioned into 1-mm-thick slices using a vibratome (VT1000S vibrating blade microtome, Leica). Fluorescence from the rhodamine within the mesh probes is visible through the tissue using a wide-field epifluorescence microscope (Olympus) when it is 50 to 100 μm from the tissue surface, which is used to adjust the sectioning such that one tissue slice includes the entire mesh probe.

After vibratome sectioning, brain slices with unmodified probes and probes modified with anti-EAAT2, anti-CD11b, IKVAV peptide, and control antibody were placed in PBS containing 4% (w/v) acrylamide (Sigma-Aldrich) and 0.25% (w/v) VA-044 thermal polymerization initiator (Thermo Fisher Scientific) at 4°C for 1 day. Brain slices with mesh probes modified with anti-D2R were placed in PBS containing 4% (w/v) acrylamide (Sigma-Aldrich) and 0.25% (w/v) VA-044 thermal polymerization initiator (Thermo Fisher Scientific) and 0.5% (w/v) paraformaldehyde at 4°C for 1 day. The brain slices were placed in freshly made acrylamide/VA-044 solution immediately before placing the brain slices in X-CLARITY polymerization system (Logos Biosystems) for 3 hours at 37°C. After polymerization, any remaining gel from the tissue surface was removed, and the slices were rinsed with PBST (PBS

with 0.2% Triton X-100; Thermo Fisher Scientific) before placing them in electrophoretic tissue clearing solution (Logos Biosystems) at 37°C for 3 to 5 days until the samples were translucent. After clearing, the brain slices were placed in fresh PBST and gently shaken for 5 hours, with the PBST replaced by fresh solution every hour. The brain slices were incubated with 1:100 to 1:200 primary antibodies—rabbit anti-NeuN (ab177487, Abcam), rat anti-GFAP (13-0300, Thermo Fisher Scientific), goat anti-Iba1 (ab5076, Abcam), and/or mouse anti-D2R conjugated to Alexa Fluor 488 (sc-5303 AF488, Santa Cruz Biotechnology)—in PBST for 4 days at 4°C with gentle shaking. After incubation, slices were placed in fresh PBST at 4°C to let excess antibody diffuse out of the tissue. The PBST was replaced with fresh solution every 8 hours over the course of 2 days. The samples were then incubated with 1:100 to 1:200 secondary antibodies—goat anti-rabbit Alexa Fluor 488 (ab150077, Abcam), goat anti-rabbit Alexa Fluor 647 (ab150079, Abcam), donkey anti-rabbit Alexa Fluor 488 (ab18723, Abcam), donkey anti-rat Alexa Fluor 647 (ab150155, Abcam), and/or donkey anti-goat Alexa Fluor 594 (ab150132, Abcam)—in PBST for 4 days at 4°C. Fluorophore-conjugated D2R primary antibody was not targeted with a secondary antibody.

Brain slices were then incubated in the refractive index matching solution of 80% glycerol:20% PBS (glycerol; Sigma-Aldrich) at least 24 hours before microscopy imaging. At least 3 hours before imaging, tissue samples were glued at their edge to the bottom of 50-mm-diameter petri dishes by Devcon 5 minute epoxy (ITW Polymers Adhesives) and then incubated in the same refractive index matching solution of 80% glycerol:20% PBS (glycerol; Sigma-Aldrich).

Microscopy imaging of brain slices

Fluorescence images were acquired on a Zeiss LSM 880 confocal microscope (Carl Zeiss Microscopy) with a 20× objective (numerical aperture of 1.0 and free working distance of 5.6 mm) or with a Zeiss Lightsheet.Z1 Microscope. Images of cleared, and immunostained brain slices were acquired using 405-, 488-, 561-, and/or 633-nm lasers as the excitation sources for Alexa Fluor 405, Alexa Fluor 488, RhBen/Alexa Fluor 594, and/or Alexa Fluor 647, respectively. The corresponding bandpass filters were 411–496, 500–553, 562–624, 624–660, and/or 677–755 nm, respectively. Confocal images were acquired by taking a tile scan together with z stacks, with a voxel size of 0.2 to 0.6 μm (x) by 0.2 to 0.6 μm (y) by 0.4 to 2.5 μm (z) and tile scan overlap of 10%. Lightsheet images were taken using a z resolution of 4 μm.

Image processing and quantification

Tile scans and z stacks of images were stitched using Zen Blue software (Zeiss). Images were then loaded into ImageJ (NIH), and channels were split and then saved into individual h5 files using Ilastik ImageJ plugin to export. The signal is then segmented in these images into individual objects by using Ilastik's pixel classification and object classification workflow (*34*, *35*). This involves manually assigning ground truth for pixels that are signal and for pixels that are not signal in individual slices of the image stack and using these assignments to teach a classifier to distinguish fluorescent labeling from noise. We trained the classifier on each channel (Iba1, NeuN, GFAP, D2R, and rhodamine mesh) in a minimum of 1000 imaging planes across several independent imaging volumes, then applied the classifier with bulk processing to the rest of the data, and generated probability masks that represent the likelihood that each pixel is signal. These probability masks were then used in the object classification workflow to separate the individual microglia, neurons, astrocytes, D2R neurons, and mesh electronics implant and then generate an information table about their center and size. MATLAB (MathWorks) was then used to quantify and plot the shortest distance of all segmented cells from the mesh electronics. Imaris (Oxford Instruments) was used to draw a virtual surface around the CA1 (fig. S26), which was then exported as an Open Microscopy Environment (OME) tiff with pixel value of 1 for the region within the surface. This CA1 tiff was then incorporated into the MATLAB code to identify which segmented cells were within the CA1 of the hippocampus.

Chronic electrophysiology recording

The electrophysiology of mice with implanted mesh probes was recorded for 10 min on days 1, 3, 5, 7, and 14 after implantation, except for those used for D2R modulation. During recording, mice were restrained in a Tailveiner restrainer (Braintree Scientific), while their head restrainers were fixed and the head-mounted FFCs were connected to an Intan RHD 2132 amplifier evaluation system (Intan Technologies) through a homemade printed circuit board. The 0–80 set screws implanted through the skull were used as reference electrodes as described previously (*12*). Electrophysiological recordings were acquired with a 20-kHz sampling rate and a 60-Hz notch filter. MATLAB (MathWorks) was used to plot and sort the spikes (*12*). Statistical analyses were performed using GraphPad Prism 9.

Modulation of D2R neuron activity

Twenty-one to 27 days after implantation, mice were anesthetized by intraperitoneal injection of a mixture of ketamine (75 mg kg^{-1}; Patterson Veterinary Supply) and dexdomitor (1 mg kg^{-1}; Orion). The degree of anesthesia was verified via toe pinch before surgery. Puralube vet ointment (Dechra Pharmaceuticals) was applied on both eyes to prevent corneal damage. A Deltaphase isothermal pad (Braintree Scientific Inc.) was heated to 39°C and placed underneath the anesthetized mouse to maintain the mouse body temperature at 37°C throughout surgery and electrophysiology recording. An alternating series of Betadine surgical scrub (Purdue Products) and 70% alcohol was applied to sterilize the skull.

A burr hole was made for intracortical drug administration according to the following stereotaxic coordinates: anteroposterior, −0.35 mm; and mediolateral, 1.45 mm (1.5 mm away from the implanted mesh probes). Drug solutions were made by dissolving D2R antagonist ETIC (2 mg in 1 ml; Sigma-Aldrich) in sterile saline. The drug solutions (10 μl) were injected 1-mm deep into the burr hole using 27-gauge needle. Before and after drug administration, neuronal activity was recorded for 20 and 30 min, respectively. After recording, the burr hole was closed by Metabond adhesive cement (Parkell), and the mouse was returned to a cage place on a 37°C heating pad. The activity of the mouse was monitored every hour until it was fully recovered from anesthesia. Buprenex (Buprenorphine, Patterson Veterinary Supply) analgesia was given intraperitoneally at a dose of 0.05 mg kg^{-1} body weight every 12 hours for up to 72 hours after surgery.

Supplementary Materials

This PDF file includes:

Figs. S1 to S26

REFERENCES AND NOTES

1. A. Mo, E. A. Mukamel, F. P. Davis, C. Luo, G. L. Henry, S. Picard, M. A. Urich, J. R. Nery, T. J. Sejnowski, R. Lister, S. R. Eddy, J. R. Ecker, J. Nathans, Epigenomic signatures of neuronal diversity in the mammalian brain. *Neuron* **86**, 1369–1384 (2015).
2. R. H. Masland, Neuronal cell types. *Curr. Biol.* **14**, R497–R500 (2004).
3. K. Sharma, S. Schmitt, C. G. Bergner, S. Tyanova, N. Kannaiyan, N. Manrique-Hoyos, K. Kongi, L. Cantuti, U.-K. Hanisch, M.-A. Philips, M. J. Rossner, M. Mann, M. Simons, Cell type–and brain region–resolved mouse brain proteome. *Nat. Neurosci.* **18**, 1819–1831 (2015).
4. M. He, Y. Liu, X. Wang, M. Q. Zhang, G. J. Hannon, Z. J. Huang, Cell-type-based analysis of microRNA profiles in the mouse brain. *Neuron* **73**, 35–48 (2012).
5. E. S. Boyden, F. Zhang, E. Bamberg, G. Nagel, K. Deisseroth, Millisecond-timescale, genetically targeted optical control of neural activity. *Nat. Neurosci.* **8**, 1263–1268 (2005).
6. J. A. Cardin, M. Carlén, K. Meletis, U. Knoblich, F. Zhang, K. Deisseroth, L.-H. Tsai, C. I. Moore, Targeted optogenetic stimulation and recording of neurons in vivo using cell-type-specific expression of Channelrhodopsin-2. *Nat. Protoc.* **5**, 247–254 (2010).
7. J. W. Salatino, K. A. Ludwig, T. D. Y. Kozai, E. K. Purcell, Glial responses to implanted electrodes in the brain. *Nat. Biomed. Eng.* **1**, 862–877 (2017).
8. R. Chen, A. Canales, P. Anikeeva, Neural recording and modulation technologies. *Nat. Rev. Mater.* **2**, 16093 (2017).
9. G. Hong, C. M. Lieber, Novel electrode technologies for neural recordings. *Nat. Rev. Neurosci.* **20**, 330–345 (2019).
10. L. Luan, J. T. Robinson, B. Aazhang, T. Chi, K. Yang, X. Li, H. Rathore, A. Singer, S. Yellapantula, Y. Fan, Z. Yu, C. Xie, Recent advances in electrical neural interface engineering: Minimal invasiveness, longevity, and scalability. *Neuron* **108**, 302–321 (2020).
11. Y. Park, T. S. Chung, G. Lee, J. A. Rogers, Materials chemistry of neural interface technologies and recent advances in three-dimensional systems. *Chem. Rev.* **122**, 5277–5316 (2022).
12. T.-M. Fu, G. Hong, T. Zhou, T. G. Schuhmann, R. D. Viveros, C. M. Lieber, Stable long-term chronic brain mapping at the single-neuron level. *Nat. Methods* **13**, 875–882 (2016).
13. T. Zhou, G. Hong, T.-M. Fu, X. Yang, T. G. Schuhmann, R. D. Viveros, C. M. Lieber, Syringe-injectable mesh electronics integrate seamlessly with minimal chronic immune response in the brain. *Proc. Natl. Acad. Sci. U.S.A.* **114**, 5894–5899 (2017).
14. X. Yang, T. Zhou, T. J. Zwang, G. Hong, Y. Zhao, R. D. Viveros, T.-M. Fu, T. Gao, C. M. Lieber, Bioinspired neuron-like electronics. *Nat. Mater.* **18**, 510–517 (2019).
15. L. Candelaria, P. N. Kalugin, B. M. Kowalski, N. G. Kalugin, Covalent epitope decoration of carbon electrodes using solid phase peptide synthesis. *Sci. Rep.* **9**, 17805 (2019).
16. M. E. Spira, A. Hai, Multi-electrode array technologies for neuroscience and cardiology. *Nat. Nanotechnol.* **8**, 83–94 (2013).
17. B. Tian, T. Cohen-Karni, Q. Qing, X. Duan, P. Xie, C. M. Lieber, Three-dimensional, flexible nanoscale field-effect transistors as localized bioprobes. *Science* **329**, 830–834 (2010).
18. Y. Zhao, S. S. You, A. Zhang, J.-H. Lee, J. Huang, C. M. Lieber, Scalable ultrasmall three-dimensional nanowire transistor probes for intracellular recording. *Nat. Nanotechnol.* **14**, 783–790 (2019).
19. Y. Gu, C. Wang, N. Kim, J. Zhang, T. M. Wang, J. Stowe, R. Nasiri, J. Li, D. Zhang, A. Yang, L. H.-H. Hsu, X. Dai, J. Mu, Z. Liu, M. Lin, W. Li, C. Wang, H. Gong, Y. Chen, Y. Lei, H. Hu, Y. Li, L. Zhang, Z. Huang, X. Zhang, S. Ahadian, P. Banik, L. Zhang, X. Jiang, P. J. Burke, A. Khademhosseini, A. D. McCulloch, S. Xu, Three-dimensional transistor arrays for intra- and inter-cellular recording. *Nat. Nanotechnol.* **17**, 292–300 (2022).
20. D. Shi, V. Dhawan, X. T. Cui, Bio-integrative design of the neural tissue-device interface. *Curr. Opin. Biotechnol.* **72**, 54–61 (2021).
21. D. O. Adewole, M. D. Serruya, J. A. Wolf, D. K. Cullen, Bioactive neuroelectronic interfaces. *Front. Neurosci.* **13**, 269 (2019).
22. K.-I. Tashiro, G. C. Sephel, B. Weeks, M. Sasaki, G. R. Martin, H. K. Kleinman, Y. Yamada, A synthetic peptide containing the IKVAV sequence from the A chain of laminin mediates cell attachment, migration, and neurite outgrowth. *J. Biol. Chem.* **264**, 16174–16182 (1989).
23. L. Kam, W. Shain, J. Turner, R. Bizios, Selective adhesion of astrocytes to surfaces modified with immobilized peptides. *Biomaterials* **23**, 511–515 (2002).
24. D. A. Heller, V. Garga, K. J. Kelleher, T.-C. Lee, S. Mahbubani, L. A. Sigworth, T. R. Lee, M. A. Rea, Patterned networks of mouse hippocampal neurons on peptide-coated gold surfaces. *Biomaterials* **26**, 883–889 (2005).
25. E. Hartfuss, R. Galli, N. Heins, M. Götz, Characterization of CNS precursor subtypes and radial glia. *Dev. Biol.* **229**, 15–30 (2001).
26. M. L. Block, L. Zecca, J.-S. Hong, Microglia-mediated neurotoxicity: Uncovering the molecular mechanisms. *Nat. Rev. Neurosci.* **8**, 57–69 (2007).
27. J. M. Lee, D. Lin, G. Hong, K.-H. Kim, H.-G. Park, C. M. Lieber, Scalable three-dimensional recording electrodes for probing biological tissues. *Nano Lett.* **22**, 4552–4559 (2022).
28. J. M. Lee, G. Hong, D. Lin, T. G. Schuhmann Jr., A. T. Sullivan, R. D. Viveros, H.-G. Park, C. M. Lieber, Nanoenabled direct contact interfacing of syringe-injectable mesh electronics. *Nano Lett.* **19**, 5818–5826 (2019).
29. J. V. Staros, R. W. Wright, D. M. Swingle, Enhancement by N-hydroxysulfosuccinimide of water-soluble carbodiimide-mediated coupling reactions. *Anal. Biochem.* **156**, 220–222 (1986).
30. S. Anbumani, A. M. da Silva, U. F. S. Roggero, A. M. P. A. Silva, H. E. Hernández-Figueroa, M. A. Cotta, Oxygen plasma-enhanced covalent biomolecule immobilization on SU-8 thin films: A stable and homogenous surface biofunctionalization strategy. *Appl. Surf. Sci.* **553**, 149502 (2021).
31. M. Zhianmanesh, A. Gilmour, M. M. M. Bilek, B. Akhavan, Plasma surface functionalization: A comprehensive review of advances in the quest for bioinstructive materials and interfaces. *Appl. Phys. Rev.* **10**, 021301 (2023).
32. T. G. Schuhmann Jr., T. Zhou, G. Hong, J. M. Lee, T.-M. Fu, H.-G. Park, C. M. Lieber, Syringe-injectable mesh electronics for stable chronic rodent electrophysiology. *J. Vis. Exp.*, e58003 (2018).
33. K. Chung, J. Wallace, S.-Y. Kim, S. Kalyanasundaram, A. S. Andalman, T. J. Davidson, J. J. Mirzabekov, K. A. Zalocusky, J. Mattis, A. K. Denisin, S. Pak, H. Bernstein, C. Ramakrishnan, L. Grosenick, V. Gradinaru, K. Deisseroth, Structural and molecular interrogation of intact biological systems. *Nature* **497**, 332–337 (2013).
34. S. Berg, D. Kutra, T. Kroeger, C. N. Straehle, B. X. Kausler, C. Haubold, M. Schiegg, J. Ales, T. Beier, M. Rudy, K. Eren, J. I. Cervantes, B. Xu, F. Beuttenmueller, A. Wolny, C. Zhang, U. Koethe, F. A. Hamprecht, A. Kreshuk, ilastik: Interactive machine learning for (bio)image analysis. *Nat. Methods* **16**, 1226–1232 (2019).
35. T. J. Zwang, B. Woost, J. Bailey, Z. Hoglund, D. S. Richardson, R. E. Bennett, B. T. Hyman, Spatial characterization of tangle-bearing neurons and ghost tangles in the human inferior temporal gyrus with three-dimensional imaging. *Brain Commun.* **5**, fcad130 (2023).
36. V. S. Polikov, P. A. Tresco, W. M. Reichert, Response of brain tissue to chronically implanted neural electrodes. *J. Neurosci. Methods* **148**, 1–18 (2005).
37. A. Marblestone, B. Zamft, Y. Maguire, M. Shapiro, T. Cybulski, J. Glaser, D. Amodei, P. B. Stranges, R. Kalhor, D. Dalrymple, D. Seo, E. Alon, M. Maharbiz, J. Carmena, J. Rabaey, E. Boyden, G. Church, K. Kording, Physical principles for scalable neural recording. *Front. Comput. Neurosci.* **7**, 137 (2013).
38. X. Wei, T. Ma, Y. Cheng, C. C. Y. Huang, X. Wang, J. Lu, J. Wang, Dopamine D1 or D2 receptor-expressing neurons in the central nervous system. *Addict. Biol.* **23**, 569–584 (2018).
39. A. R. West, A. A. Grace, Opposite influences of endogenous dopamine D1 and D2 receptor activation on activity states and electrophysiological properties of striatal neurons: Studies combining in vivo intracellular recordings and reverse microdialysis. *J. Neurosci.* **22**, 294–304 (2002).
40. S. Robinson, D. M. Smith, S. J. Mizumori, R. D. Palmiter, Firing properties of dopamine neurons in freely moving dopamine-deficient mice: Effects of dopamine receptor activation and anesthesia. *Proc. Natl. Acad. Sci. U.S.A.* **101**, 13329–13334 (2004).
41. D. Chen, J. Li, Interfacial design and functionization on metal electrodes through self-assembled monolayers. *Surf. Sci. Rep.* **61**, 445–463 (2006).
42. J. G. Hensler, in *Basic Neurochemistry*, G. J. Siegel, R. W. Albers, S. T. Brady, D. L. Price, Eds. (Elsevier Academic Press, 2007), chap. 13, pp. 227–248.
43. A. Cioce, B. Calle, T. Rizou, S. C. Lowery, V. L. Bridgeman, K. E. Mahoney, A. Marchesi, G. Bineva-Todd, H. Flynn, Z. Li, O. Y. Tastan, C. Roustan, P. Soro-Barrio, M.-R. Rafiee, A. Garza-Garcia, A. Antonopoulos, T. M. Wood, T. Keenan, P. Both, K. Huang, F. Parmeggian, A. P. Snijders, M. Skehel, S. Kjær, M. A. Fascione, C. R. Bertozzi, S. M. Haslam, S. L. Flitsch, S. A. Malaker, I. Malanchi, B. Schumann, Cell-specific bioorthogonal tagging of glycoproteins. *Nat. Commun.* **13**, 6237 (2022).
44. A. Kataki-Anastasakou, S. Hernandez, E. M. Sletten, Cell-surface labeling via bioorthogonal host–guest chemistry. *ACS Chem. Biol.* **16**, 2124–2129 (2021).
45. G. T. Hermanson, *Bioconjugate Techniques* (Academic Press, ed. 3, 2013).
46. K. Deisseroth, Optogenetics: 10 Years of microbial opsins in neuroscience. *Nat. Neurosci.* **18**, 1213–1225 (2015).
47. K. M. Tye, K. Deisseroth, Optogenetic investigation of neural circuits underlying brain disease in animal models. *Nat. Rev. Neurosci.* **13**, 251–266 (2012).

Acknowledgments

Funding: This work was supported by Air Force Office of Scientific Research FA9550-18-1-0469 (C.M.L), Lieber Research Group (C.M.L.), American Heart Association 23POST1018301 (A.Z.), National Institutes of Health K99AG068602 (T.J.Z.), and Harrison Gardner, Jr. Award (T.J.Z.). This work was performed, in part, at the Harvard University Center for Nanoscale Systems (CNS), a member of the National Nanotechnology Coordinated Infrastructure Network (NNCI), which is supported by the National Science Foundation under NSF award no. ECCS-2025158. We thank

the Harvard Center for Biological Imaging (RRID:SCR_018673) for infrastructure and support.
Author contributions: Conceptualization: A.Z., T.J.Z., and C.M.L. Methodology: A.Z., T.J.Z., and C.M.L. Investigation: A.Z., T.J.Z., and C.M.L. Visualization: A.Z. and T.J.Z. Funding acquisition: C.M.L., A.Z., and T.J..Z. Project administration: C.M.L. Supervision: C.M.L. Writing—original draft: A.Z., T.J.Z., and C.M.L. Writing—review and editing: A.Z., T.J.Z., and C.M.L. **Competing interests:** The authors declare that they have no competing interests. **Data and materials availability:** All data needed to evaluate the conclusions in the paper are present in the paper and/or the Supplementary Materials.

Submitted 2 August 2023
Accepted 30 October 2023
Published 29 November 2023
10.1126/sciadv.adk1050